Research Article | Vol. 26, No. 25 | 10 Dec 2018 | OPTICS EXPRESS 33440
Optics EXPRESS

Carrier-envelope phase-dependent molecular high-order harmonic generation from H_2^+ in a multi-cycle regime

BAONING WANG,[1] LIXIN HE,[1,*] HUA YUAN,[1] QINGBIN ZHANG,[1,3] PENGFEI LAN,[1,4] AND PEIXIANG LU[1,2]

[1] *Wuhan National Laboratory for Optoelectronics and School of Physics, Huazhong University of Science and Technology, Wuhan 430074, China*
[2] *Hubei Key Laboratory of Optical Information and Pattern Recognition, Wuhan Institute of Technology, Wuhan 430205, China*
[3] *zhangqingbin@mail.hust.edu.cn*
[4] *pengfeilan@mail.hust.edu.cn*
[*] *helx@mail.hust.edu.cn*

Abstract: Carrier-envelope phase (CEP) dependence of high-order harmonic generation (HHG) from H_2^+ in a multi-cycle laser pulse is investigated by solving the non-Born-Oppenheimer time-dependent Schrödinger equation (TDSE). It is found that high harmonics in the plateau exhibit counterintuitive frequency modulation (FM) as the CEP of the multi-cycle laser varies. Based on the classical electron trajectories and time-frequency analysis, this multi-cycle CEP-dependent FM is demonstrated to result from the interference of half-cycle HHG radiations, which is modulated by laser-driven nuclear motion. The mechanism of the CEP-dependent FM is further confirmed by simulations based on a simple algorithm in the time domain, which satisfactorily reproduces the TDSE results. The CEP-dependent FM encodes rich information on the correlated electron and nuclear dynamics, which paves the way for probing nuclear motion with attosecond resolution.

1. Introduction

High-order harmonic generation (HHG) through laser-matter interaction is considered to be essential for tabletop sources of the extreme ultraviolet (XUV) to soft x-ray radiation [1–3] and attosecond (1 as = 10^{-18} s) pulses [4–6]. Moreover, HHG is also an important tool to probe the structure and electron dynamics in atoms, molecules and solid with unprecedented resolution [7–17], since rich information is encoded in the amplitude, frequency, phase, and polarization of the harmonic emission during the laser-mater interaction [18–32]. For these potential applications, HHG has been a topic of great interest in the past two decades.

The mechanism of HHG can be understood by the semiclassical three-step model: removal of an electron by an intense laser pulse, acceleration of the electron in laser field, and recombination with the parent ion [33, 34]. In temporal domain, this process repeats every half optical cycle and pulsed radiations are generated during the process. The radiation within each half-cycle defines a series of temporal slits and constitutes a multi-slit interferometer. The total emission is a coherent superposition of these half-cycle radiations. In spectral domain, this interference results in a comb of harmonics in the plateau. Resolving two neighboring harmonics is equivalent to the detection of a single fringe. In this context, the carrier-envelope phase (CEP), a critical parameter of ultrashort laser pulses, directly determines the laser waveform within each half optical cycle. The variation of CEP will therefore modulate the half-cycle radiations and then make a difference in the harmonic spectrum [35–40]. To date, the CEP effect has been widely studied in HHG from atoms. For instance, by using 5-fs CEP-stabilized laser system, Baltuška

#347524 https://doi.org/10.1364/OE.26.033440
Journal © 2018 Received 4 Oct 2018; revised 18 Nov 2018; accepted 19 Nov 2018; published 7 Dec 2018

Optics EXPRESS

et al. found the CEP-dependent frequency shift of the harmonics in the cutoff region [35–37]. Haworth *et al*. also demonstrated that the CEP can significantly influence half-cycle cutoffs in harmonic spectra [38]. Recently, the CEP-dependent HHG has been extended to the mid-infrared regime to generate soft X-ray attosecond pulses [39]. However, the CEP effects are expected to be inessential for multi-cycle driving lasers.

Recently, molecular high-order harmonic generation (MHOHG) has attracted widespread attention. Compared to atoms, MHOHG exhibits some more interesting features, such as the structure or dynamic minimum [41–43], the shape resonance [44], and so on. More than that, the laser-driven nuclear motion in molecules can also influence the electron dynamics and then the HHG. Zuo and Bandrauk has demonstrated that charge-resonance-enhanced ionization (CREI) [45,46] will occur at large internuclear distance, which will result in the amplitude [18–22] and frequency [23–25] modulations in HHG. These effects, in turn, can be used to retrieve the information of molecular structure and nuclear dynamics.

In this paper, we theoretically investigate CEP effect on HHG from H_2^+ in a multi-cycle laser pulse by numerically solving the non-Born-Oppenheimer (non-BO) time-dependent Schrödinger equation (TDSE). A multi-cycle frequency modulation (FM) of high harmonics in the plateau is observed as the CEP varies. Such a multi-cycle CEP effect, however, has never been observed in HHG from noble-gas atoms. Our simulations based on the classical electron trajectories and time-frequency analysis indicate that the CEP-dependent multi-cycle FM mainly arises from the interference of the half-cycle radiations in HHG, which is modulated by the CREI induced by laser-driven nuclear motion. By using a simple algorithm of this temporal interference, we reproduce the CEP-dependent FM in HHG from H_2^+. The CEP-dependent FM reveals the temporal information of HHG from moving H_2^+ and is potential for retrieving the nuclear dynamics with attosecond resolution.

2. Theoretical model

We investigate HHG from H_2^+ by numerically solving the non-BO TDSE, which consists of one-dimensional motion of nuclei and one-dimensional motion of electron. In our simulation, the H_2^+ molecular ion is assumed to be aligned along the polarization direction of the linearly polarized laser pulses. The TDSE is expressed as [47, 48] (Hartree atomic units are used throughout):

$$i\frac{\partial}{\partial t}\psi(R,z;t) = [H_0 + V(t)]\psi(R,z;t), \tag{1}$$

where H_0 is the field-free Hamiltonian:

$$\begin{aligned} H_0 =& T + V_0 \\ =& -\frac{1}{2\mu}\frac{\partial^2}{\partial R^2} - \frac{1}{2\mu_e}\frac{\partial^2}{\partial z^2} - \frac{1}{\sqrt{(z-R/2)^2+\alpha}} - \frac{1}{\sqrt{(z+R/2)^2+\alpha}} + \frac{1}{\sqrt{R^2+\beta}}. \end{aligned} \tag{2}$$

Here, R is the internuclear distance, z is the electron position measured from the center-of-mass of two protons, $\mu = m_p/2$ and $\mu_e = 2m_p/(2m_p + 1)$ are the reduced masses (m_p is the mass of the proton). $\alpha = 1$ and $\beta = 0.03$ are the soft-core parameters. In the dipole approximation, the length-gauged laser-molecule interaction is $V(t) = [1 + 1/(2m_p + 1)]zE(t)$. $E(t) = E_0 sin^2(\pi t/\tau)cos(\omega t + \phi_0)$ is the laser field. E_0, ω, and ϕ_0 are the amplitude, frequency, and CEP of this field. τ is the pulse duration. In our simulation, an 800-nm laser pulse with the intensity of 3×10^{14} W/cm^2 and total duration of 20 optical cycles is adopted. We solve Eq. (1) by using the Crank-Nicolson method [47,48]. To eliminate artificial reflections from boundaries, the wave function is multiplied by a $sin^{1/6}$-masking function at each time step. The initial

Optics EXPRESS

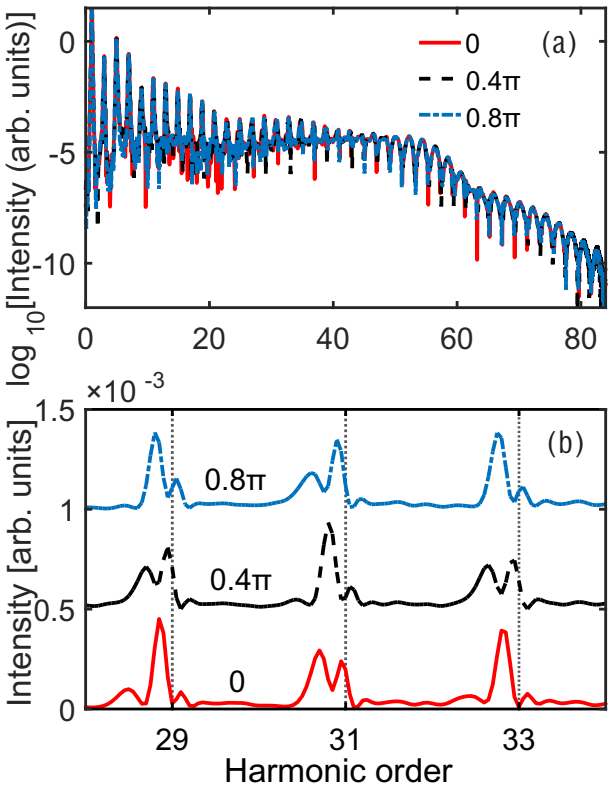

Fig. 1. (a) Harmonic spectra of moving H_2^+ with the CEP of 0 (solid line), 0.4π (dashed line), 0.8π (dash-doted line). (b) Same as (a), but for the results of H29-H33. For clarity, the intensities of these three harmonics are plotted in linear scale and shifted vertically.

state is the ground state $1s\sigma_g$ of H_2^+, which is obtained by using imaginary time propagation method of the field-free TDSE. Its energy is -0.78 a.u. and the equilibrium internuclear distance is $R_e = \frac{\langle\psi_0|R|\psi_0\rangle}{\langle\psi_0|\psi_0\rangle} = 2.6$ a.u. (ψ_0 is the initial wavefunction). Harmonic spectrum is obtained by the Fourier transformation of the dipole acceleration $a(t) = \langle\psi(t)| - \frac{\partial V_0}{\partial z} + E(t)|\psi(t)\rangle$. For comparison, we also solve Eq. (1) with the internuclear distance fixed at R_e, which is called the static case in the following.

It should be emphasized that the most accurate way to model the HHG process is by solving the 3D TDSE. While in our case, we use a linearly polarized driving laser. The dynamics of the electron and nuclei are mainly along the polarization direction of the laser field. Therefore, it is justified to model the HHG with the 1D TDSE. Compared to the 3D model, the 1D result may lose some effects, such as the transversal spreading of the electron wave packet [49]. These effects, however, become important only when the laser wavelength is long, e.g., in the mid-infrared band. For an 800 nm near-infrared laser used in our simulations, these effects are very weak. Moreover, these effects primarily affect the harmonic yields, which will not severely alter the FM in HHG discussed here.

3. Results and discussions

In Fig. 1(a), we present the harmonic spectra calculated by solving the non-BO TDSE (moving H_2^+) for three different CEPs. The harmonic spectra exhibit clear separated harmonic peaks. In this work, we mainly focus on the harmonics in the plateau. In Fig. 1(b), we show the results

Optics EXPRESS

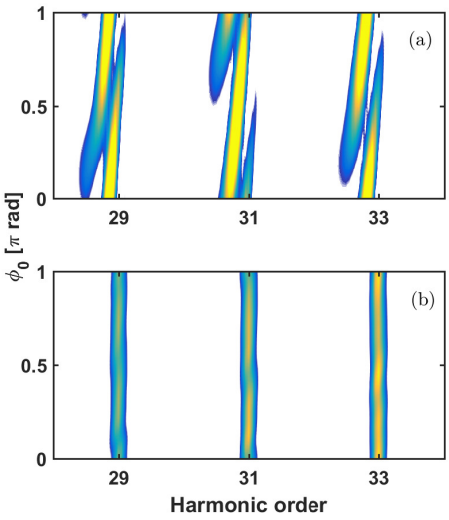

Fig. 2. (a) The CEP-dependent spectra of H29-H33 for moving H_2^+. (b) Same as (a), but for static H_2^+.

of the 29th-33rd harmonics (H29-H33). One can see that all these harmonics are substantially redshifted. More importantly, as the CEP varies, the harmonics are split and exhibit some complicated spectral structures. For clarity, we have calculated the harmonic spectra as a function of the laser CEP. The results of H29-H33 are shown in Fig. 2(a). For comparison, the results of HHG from static H_2^+ (a case similar to atoms) are also presented in Fig. 2(b). It's obvious that the spectral distribution of each harmonic from moving H_2^+ exhibits a series of diagonal stripes. While for static H_2^+, the harmonic spectra are composed by several typical odd harmonics. The spectral structures of these harmonics are regular and nearly unchanged with the CEP.

To gain insight into the complex spectral distribution in HHG from moving H_2^+, we next investigate the temporal emission of the harmonics by performing the time-frequency analysis. Figure 3(a) shows the result of H31 from moving H_2^+. For clarity, the results for CEP=0, 0.2π, and 0.8π are presented in Fig. 3(b). One can see that the temporal profile of H31 exhibits two main emission events located in vicinity of $10T_0$ and $14T_0$, respectively. Note that, the central part of the laser pulse in our simulations is $10T_0$ and therefore the emission near $10T_0$ is mainly due to the highest intensity of the laser field. In contrast, the dominant emission near $14T_0$ locates on the falling part of the laser field and can be understood as a consequence of the laser-driven nuclear motion. The nuclear motion in H_2^+ is mainly initiated by the laser-induced ionization of the electron, which breaks the balance of the electric field force within H_2^+. After the ionization, the repulsive force between the two nuclei drives the molecule to dissociate and then leads to the rapid nuclear motion [23]. The nuclear wave packet forced by the laser field could go beyond the equilibrium internuclear distance and move toward larger internuclear distance [see Process 2 in Fig. 4(a)], where the ionization rate is higher than that at the equilibrium internuclear distance due to the smaller ionization potential [see Process 3 in Fig. 4(a)]. As shown in Fig. 4(b), the increasing internuclear distance leads to an enhancement of ionization and therefore dominant harmonic emission at the falling edge of the laser field. In contrast, the nuclear wave packet is restricted to the equilibrium internuclear distance for static H_2^+, [see Process 1 in Fig. 4(a)]. Therefore, the main emission for static H_2^+ mainly occurs in the vicinity of $10T_0$ [see Fig. 3(c) and 3(d)], i.e., at the central part of the laser field, where the electric field is the highest. Note that, nuclear motions are almost identical for all the CEPs [see Fig. 4(b)]. This rules out the

Optics EXPRESS

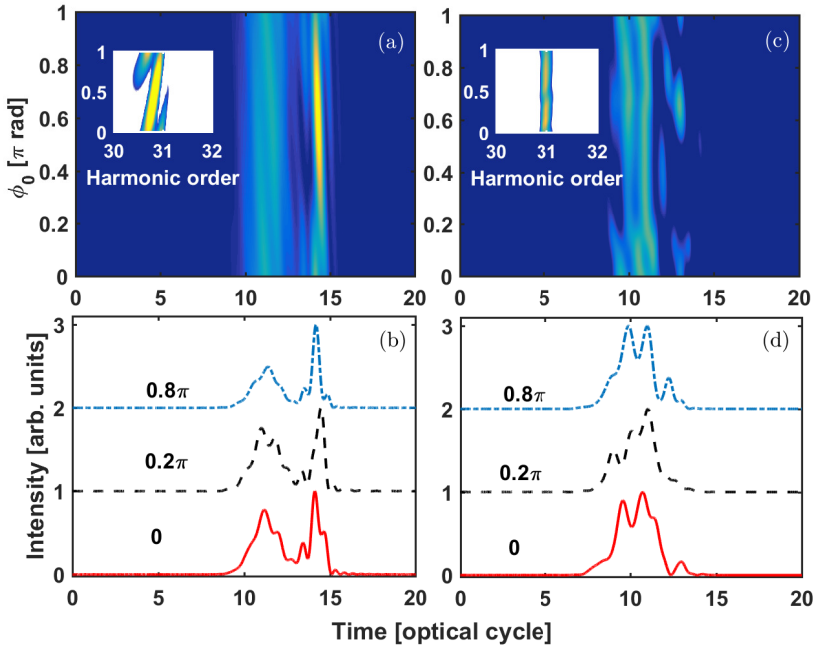

Fig. 3. (a) Temporal profile of H31 from moving H_2^+ as a function of the CEP. The inset illustrates CEP-dependent spectra of H31. (b) Temporal profile of H31 from moving H_2^+ with the CEP of 0 (solid line), 0.2π (dashed line), 0.8π (dash-doted line). For clarity, the profiles of these cases have been shifted vertically. (c) and (d) Same as (a) and (b), but for static H_2^+.

possibility of the CEP-dependent variation of $\langle R(t)\rangle$ that causes the complex spectral distribution in Fig. 2(a).

We have also analyzed the classical electron trajectories of HHG from the moving H_2^+. Figures 5(a)-(c) show the classical electron kinetic energies as a function of the emission time in the case of CEP = 0, 0.4π, and 0.8π, respectively. Here, only the results for two main emission events near $10T_0$ and $14T_0$ are presented. As can be seen from Fig. 5, the time delay between two adjacent half-cycle radiations are different for these two emission events. Moreover, this time delay for each event depends on the laser CEP. Quantitatively, we have plotted in Fig. 6 the time delay as a function of the CEP for H31 for these two emission events. It's obvious that the time delays of the two adjacent half-cycle radiations in the vicinity of $10T_0$ are very close to $0.5T_0$ (0.502-$0.500T_0$). While in the vicinity of $14T_0$, the delays are much larger (0.526-$0.519T_0$). It has been reported that the time delay of $0.5T_0$ just corresponds to the consecutive interference of odd harmonics [33, 34, 50, 51]. A larger (smaller) time delay means that the consecutive interference between two adjacent emissions occurs at a slightly lower (higher) frequency, leading to a redshift (blueshift) of the harmonic [50, 51]. For moving H_2^+, the harmonic emission is dominated at $14T_0$ where the time delay is larger than $0.5T_0$. Therefore, the generated harmonics show global redshift [Fig. 2(a)]. Moreover, the decreasing CEP-dependent time delay is responsible for the blueshift of those diagonal stripes therein. While for static H_2^+, harmonic emission mainly occurs at $10T_0$ where the time delay is very close to $0.5T_0$, which therefore leads to a series of typical odd harmonics.

In the following, we demonstrate that the CEP-dependent FM in HHG from moving H_2^+ is

Optics EXPRESS

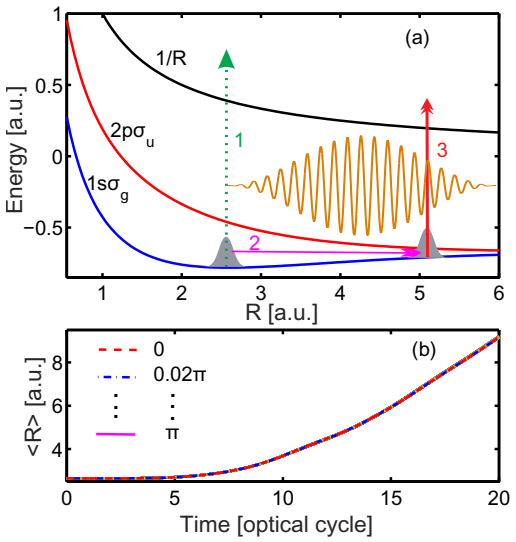

Fig. 4. (a) Mechanism of HHG from moving H_2^+. For static H_2^+, the ionization occurs at the equilibrium distance (Process 1). For moving H_2^+, the nuclear wave packet is forced to larger internuclear distance (Process 2) and then the ionization occurs with a lower ionization threshold (Process 3). (b) Time-dependent internuclear distance $\langle R(t)\rangle$ calculated for different CEPs.

due to temporal interference of the two emission events at $10T_0$ and $14T_0$. As mentioned above, HHG can be understood as a coherent superposition of each half-cycle radiation during the laser pulse [40], i.e.,

$$S(\omega;\phi_0) = |\Sigma A_n(\omega)e^{i(\omega t_n+\phi_n)}|^2. \tag{3}$$

Here, t_n is the emission time of each radiation, which can be calculated from the three-step model. $\phi_n = U_p\tau_n$ is the phase of the emission, τ_n is the excursion time of the return electrons in the acceleration step [33, 34]. A_n represents the amplitude of each radiation. Note that the most crucial factor that determines the interference pattern (i.e., the CEP-dependent FM) is the relative phase of these radiations. The amplitudes A_n just make a difference in the intensity of each frequency component of the modulated harmonics, but will not change the CEP dependence. For simplicity, we have set A_n to 1 for each radiation. Based on this temporal algorithm, we have simulated the generation of H31 from moving H_2^+ by considering two pairs of consecutive radiation events in the vicinity of $10T_0$ and $14T_0$. The results are presented in Fig. 7(a). One can see that, the main feature of the CEP-dependent FM is well reproduced. For comparison, the result from static H_2^+ is also simulated by using one pair of consecutive emission events at $10T_0$. As shown in Fig. 7(b), the result also agrees with the TDSE simulations in Fig. 2(b). Note that the calculated harmonic in Fig. 7(b) shows a little bit of blueshift as the CEP varies due to the slight decrease of the CEP-dependent time delays at $10T_0$ (see dashed line in Fig. 6). Considering the simplicity of this temporal algorithm, the agreement of the results in Fig. 7 with the TDSE simulations in Fig. 2 is satisfying.

It's worth mentioning that, apart from the CREI effect, the nuclear motion could also lead to the electron localization in the HHG process. It has been reported that the electron localization will break the symmetry of the electron density and then lead to the emission of even harmonics [52–56]. In that case, the electron localization mainly controls the interference of the emissions from the successive laser half-cycles. While in our work, the FM in HHG mainly arises from the interference of two separated emission events: one occurs at the central part of the laser

Optics EXPRESS

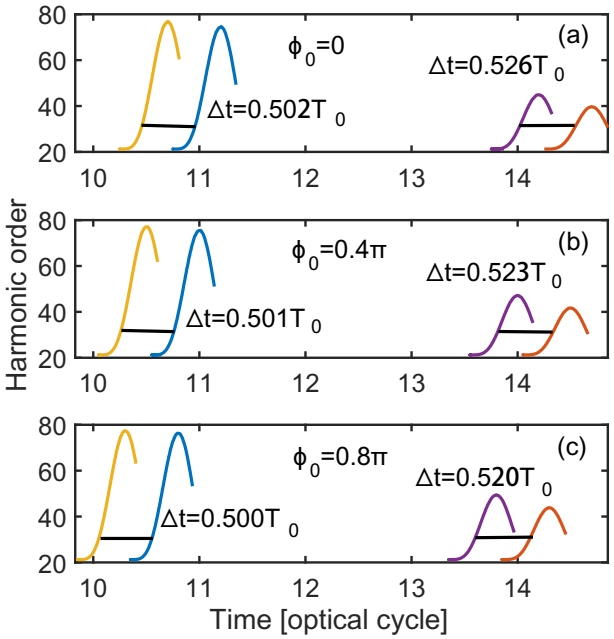

Fig. 5. The classical electron kinetic energy as a function of the emission time for ϕ_0 = (a) 0, (b) 0.4π, (c) 0.8π. The energy corresponding to H31 is indicated as the horizontal lines and the time delays Δt between two consecutive emissions for H31 are also illustrated.

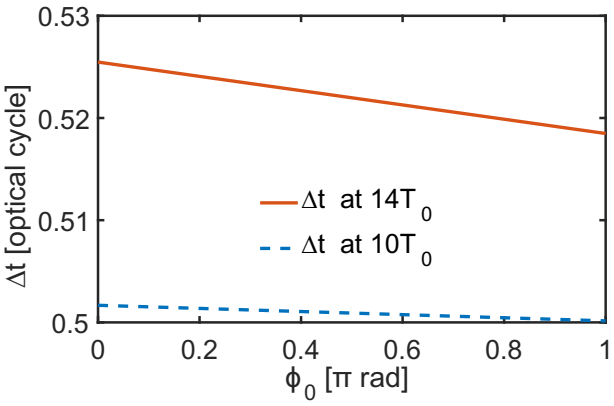

Fig. 6. Time delays between two consecutive emissions near $14T_0$ (red solid line) and $10T_0$ (blue dashed line) as a function of the laser CEP.

field due to the peak laser intensity, the other one occurs at the falling part of the laser field due to nuclear motion induced CREI. The interference pertains to a longer time-scale and hence gives rise to fine modifications in the harmonic spectrum within the width of odd-order harmonics, but will not turn odd harmonics into even [54]. Besides, it can be expected that the CEP-dependent FM will disappear in the monochromatic limit, since the long time-scale interference mentioned above will not happen. This is because in the monochromatic limit, the laser intensity are nearly the same throughout the pulse, there will be only one dominant HHG event resulting from the CREI. Note that the fine modulations have also been observed in HHG from alkali atoms [57], where the modulations are demonstrated to arise from the complex dynamics of the ground state

Optics EXPRESS

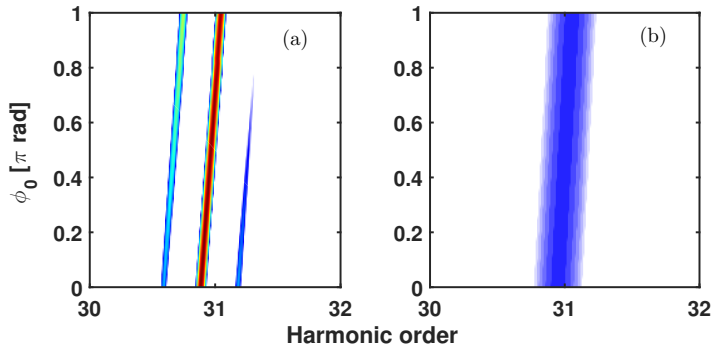

Fig. 7. (a) The spectra of H31 from moving H_2^+ reproduced by Eq.(4). (b) Same as (a), but for the static H_2^+.

population induced by the Rabi-Flopping at the resonant laser wavelength, which is different from the interference mechanism discussed here.

Next, we investigate the influence of the laser intensity on the CEP-dependent FM in HHG from H_2^+. Figure 8 shows the results for the laser intensity of 1.5×10^{14}W/cm^2, 2.5×10^{14}W/cm^2, 3.5×10^{14}W/cm^2, and 4.5×10^{14}W/cm^2, respectively. Since the bandwidth of the harmonic plateau will increase with the laser intensity, for better comparison, we mainly focus on the result of the harmonic with the photon energy of $I_p + 1.5U_p$ for each laser intensity. Here I_p is the ionization potential of H_2^+, U_p is the ponderomotive energy. As shown in the left panels of Fig. 8, the CEP-dependent FM is observed for the laser intensity of 2.5×10^{14}W/cm^2 [Fig. 8(c)] and 3.5×10^{14}W/cm^2 [Fig. 8(e)], but disappears for 1.5×10^{14}W/cm^2 [Fig. 8(a)] and 4.5×10^{14}W/cm^2 [Fig. 8(g)]. To understand this phenomenon, we have calculated the Gabor profiles for the harmonics presented in the left panels. Corresponding results are shown in the right panels. One can see that, with laser intensity as low as 1.5×10^{14}W/cm^2 [Fig. 8(b)], the harmonic emission at the central part of the laser field is rather weak due to the low ionization. The dominant emission mainly occurs on falling part where the molecule is already stretched. In this case, the long time-scale interference will not happen. The harmonic emission is mainly a consequence of the interference of the successive half-cycle bursts at the falling part, which therefore does not lead to apparent FM in the harmonic spectrum. While for a much higher laser intensity of 4.5×10^{14}W/cm^2, the harmonic emission at the falling part of the electric field is severely reduced due to serious depletion of the ground state within such an intense laser pulse. The dominant emission only occurs at central part of the field [see Fig. 8(h)]. This case is similar to that in Fig. 3(c). Therefore, the FM is also invisible in this case. For the moderate intensities of 2.5×10^{14}W/cm^2 and 3.5×10^{14}W/cm^2 [see Fig. 8(d) and 8(f)], one can see two obvious emission events located at the central and falling parts of the laser field ($11.5T_0$ and $14T_0$ for 2.5×10^{14}W/cm^2 and $10.5T_0$ and $14.5T_0$ for 3.5×10^{14}W/cm^2). The interference of these two separated events will therefore lead to the FM shown in Fig. 8(b) and 8(c). From the above, we conclude that to achieve the long time-scale interference and therefore the CEP-dependent FM, the laser intensity should be properly adopted so that the nuclear motion as well as the harmonic process can be well controlled.

Finally, we demonstrate that the CEP-dependent FM in HHG from moving H_2^+ can be used to retrieve the nuclear dynamics with attosecond resolution. It has been reported that the nonadiabatic effect of the time-dependent laser intensity can induce a red (blue) shift when HHG

Optics EXPRESS

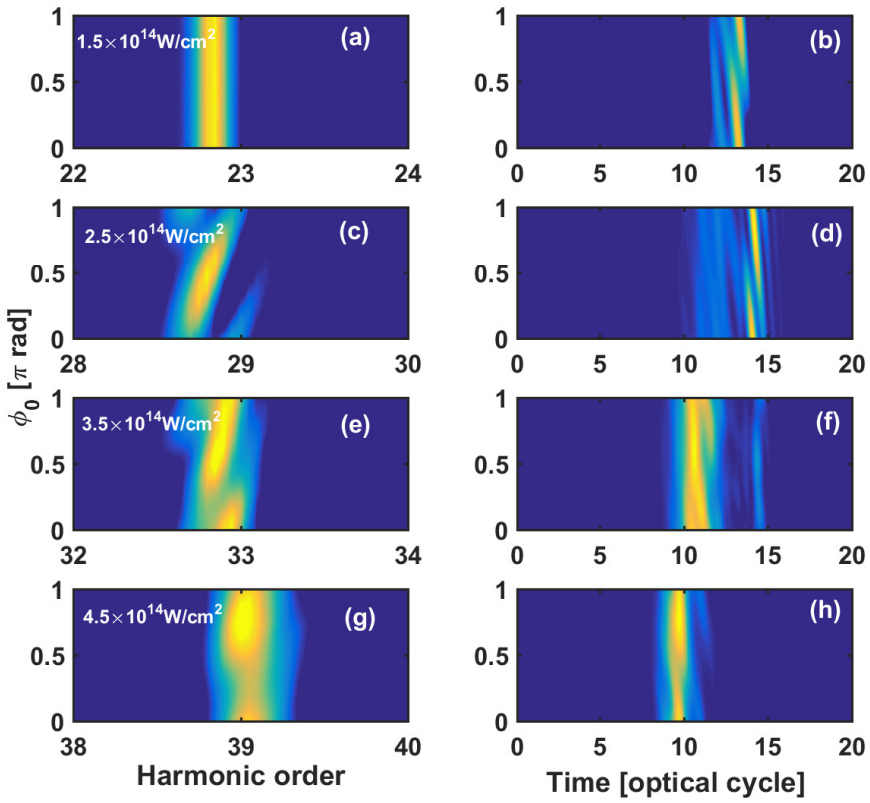

Fig. 8. Left panels: CEP-dependent FM in HHG from H_2^+ with the laser intensity of 1.5×10^{14}W/cm^2, 2.5×10^{14}W/cm^2, 3.5×10^{14}W/cm^2, 4.5×10^{14}W/cm^2, respectively. Right panels: CEP-dependent temporal profiles of the harmonics presented in the left panels.

is dominant at the falling (raising) part of the laser pulse. The frequency shift is given by:

$$\Delta\omega = \alpha_q \frac{\partial I(t)}{\partial t}|_{t_d}, \tag{4}$$

where α_q is the phase coefficient of the harmonic, $I(t)$ is the laser intensity, and t_d is the emission time of the dominant HHG. As discussed above, the CEP-dependent FM reveals temporal information of HHG. Using Eq. (3), one can extract the emission time t_d of HHG dominated at the falling edge of the laser pulse from the CEP-dependent FM (it's about $14T_0$ in our work). Moreover, for moving H_2^+, the nonadiabatic frequency shift can be related to the ionization asymmetry induced by nuclear motion [23], i.e.,

$$\frac{\Delta\omega}{\omega} = \frac{\Gamma(R_r, I) - \Gamma(R_f, I)}{2\Gamma(R_e, I)}. \tag{5}$$

Here, Γ is the ionization rate, which is nearly linearly dependent on R before it reaches R_c [45,46]. R_r and R_f are the mean internuclear distances on the rising and falling part of the laser field. Under our laser conditions, the nuclear motion on the raising part of the laser field is small [as illustrated in Fig. 4(b)], namely, $R_r \approx R_e$. Then the frequency shift of the dominant HHG can be

Optics EXPRESS

evaluated by

$$\frac{\Delta\omega}{\omega} \approx \frac{R_e - R_f}{2R_e}. \tag{6}$$

Combining the Eqs. (4) and (6), the internuclear distance of H_2^+ can be roughly retrieved. For instance, the emission of H31 at CEP=0 is dominated at $14.1T_0$ [see Fig. 3(a)], where the frequency shift predicted by Eq. (4) is about -0.58ω (The minus sign means a red shift). Inserting this frequency shift into Eq. (6), we can then get the internuclear distant at the emission time, i.e., about 5.6 a.u. This result agrees well with the TDSE prediction (about 5.4 a.u.) in Fig. 4(b). Moreover, as shown in Fig. 3(a), the variation of CEP will change the emission time of the falling part HHG. While the nuclear dynamics are nearly unchanged as the CEP varies [see Fig. 4(b)]. This allows one to build a one-to-one map between the internuclear distance with the emission time of HHG via the CEP-dependent nonadiabatic frequency shift and then achieve the real-time measurement of the nuclear motion. According to the three-step model [33, 34], a π shift in the CEP will lead to a change of $0.5T_0$ in the emission time of HHG. With the CEP changing with a step of 100 mrad (which can be achieved in experiment), one can realize a 43 as resolution in time. Therefore, our work can pave a way for probing the nuclear motion with attosecond resolution.

In experiment, the phase-matching usually plays an important role in macroscopic harmonic generation. Especially, some propagation effects, like the self-phase modulation of the fundamental beam within the gas medium [58], will also lead to a frequency shift in HHG, which may cover up the FM predicted in our work. However, the phase-matching effects can be controlled by adjusting the experimental conditions. It has also been reported that by using a thin gas jet with low gas pressure, the collective effects can be effectively minimized and the macroscopic harmonic emission can agree well with the simulations of individual response [59–61]. More recently, the nuclear motion induced frequency shift in HHG from H_2/D_2 has been observed in experiment [25]. Under suitable experimental conditions, we believe that our results can also be demonstrated in experiment.

4. Conclusion

In conclusion, the CEP effect in HHG from H_2^+ in a multi-cycle laser pulse is theoretically investigated by solving the non-BO TDSE. The results show that harmonics in the plateau from the moving H_2^+ are substantially redshifted and complicated spectral structures are observed as the laser CEP varies. In contrast, HHG from the static H_2^+ exhibits typical odd harmonic peaks. Based on the classical electron trajectories and time-frequency analysis, we find that the CEP-dependent FM in HHG from moving H_2^+ is attributed to the temporal interference of two radiation events located in the vicinity of $10T_0$ and $14T_0$, respectively. Compared to static H_2^+, the extra radiation at $14T_0$ mainly arises from the CREI effect induced by the laser-driven nuclear motion of moving H_2^+. Our above analysis is further confirmed by simulations based on a simple algorithm of the temporal interference, which well reproduces the main feature of the CEP-dependent spectral structures of HHG. Moreover, we demonstrate the nuclear dynamics of H_2^+ can be retrieved from the CEP-dependent FM in HHG with attosecond resolution.

Funding

National Natural Science Foundation of China (No. 11627809, 11874165, 11704137, 11774109); the Program for HUST Academic Frontier Youth Team.

Optics EXPRESS

References

1. M.-C. Chen, P. Arpin, T. Popmintchev, M. Gerrity, B. Zhang, M. Seaberg, D. Popmintchev, M. M. Murnane, and H. C. Kapteyn,"Bright, coherent, ultrafast soft x-ray harmonics spanning the water window from a tabletop light source," Phys. Rev. Lett. **105**, 173901 (2010).
2. E.J. Takahashi, T. Kanai, K. L. Ishikawa, Y. Nabekawa, and K. Midorikawa, "Coherent water window x-ray by phase-matched high-order harmonic generation in neutral media," Phys. Rev. Lett. **101**, 253901 (2008).
3. T. Popmintchev, M.-C. Chen, D. Popmintchev, P. Arpin, S. Brown, S. Ališauskas, G. Andriukaitis, T. Balčiunas, O. D. Mücke, A. Pugzlys, A. Baltuška, B. Shim, S. E. Schrauth, A. Gaeta, C. Hernández-García, L. Plaja, A. Becker, A. Jaron-Becker, M. M. Murnane, H. C. Kapteyn, "Bright coherent ultrahigh harmonics in the keV X-ray from mid-infrared femtosecond lasers," Science **336**, 1287-1291 (2012).
4. E. Goulielmakis, M. Schultze, M. Hofstetter, V. S. Yakovlev, J. Gagnon, M. Uiberacker, A. L. Aquila, E. M. Gullikson, D. T. Attwood, R. Kienberger, F. Krausz, and U. Kleineberg, "Single-cycle nonlinear optics," Science **320**, 1614-1617 (2008).
5. J. Li, X. Ren, Y. Yin, K. Zhao, A. Chew, Y. Chang, E. Cunningham, Y. Wang, S. Hu, Y. Wu, M. Chini, and Z. Chang, "53-attosecond X-ray pulses reach the carbon K-edge," Nat. Commun. **8**, 186 (2017).
6. T. Gaumnitz, A. Jain, and H. J. Wörner, "Complete reconstruction of ultra-broadband isolated attosecond pulses including partial averaging over the angular distribution," Opt. Express **26**, 14719-14740 (2018).
7. J. Itatani, J. Levesque, D. Zeidler, H. Niikura, H. Pépin, J. C. Kieffer, P. B. Corkum, and D. M. Villeneuve, "Tomographic imaging of molecular orbitals," Nature (London) **432**, 867-871 (2004).
8. H. Yuan, L. He, F. Wang, B. Wang, X. Zhu, P. Lan, and P. Lu, "Tomography of asymmetric molecular orbitals with a one-color inhomogeneous field," Opt. Lett. **43**, 931-934 (2018).
9. R. Kienberger, M. Hentschel, M. Uiberacker, C. Spielmann, M. Kitzler, A. Scrinzi, M. Wieland, T. Westerwalbesloh, U. Kleineberg, U. Heinzmann, M. Drescher, and F. Krausz, "Steering attosecond electron wave packet with light," Science **297**, 1144-1148 (2002).
10. M. Uiberacker, T. Uphues, M. Schultze, A. J. Verhoef, V. Yakovlev, M. F. Kling, J. Rauschenberger, N. Kabachnik, H. Schroeder, M. Lezius, K. L. Kompa, and H.-G. Muller, "Attosecond real-time observation of electron tunneling in atoms," Nature (London) **446**, 627-632 (2007).
11. P. M. Kraus, B. Mignolet, D. Baykusheva, A. Rupenyan, L. Horný, E. F. Penka, G. Grassi, O. I. Tolstikhin, J. Schneider, F. Jensen, L. B. Madsen, A. D. Bandrauk, F. Remacle, and H. J. Wörner, "Measurement and laser control of attosecond charge migration in ionized iodoacetylene," Science **350**, 790-795 (2015).
12. L. He, P. Lan, A.-T. Le, B. Wang, B. Wang, X. Zhu, P. Lu, and C. D. Lin, "Real-time observation of molecular spinning with angular high-harmonic spectroscopy," Phys. Rev. Lett. **121**, 163201 (2018).
13. X. Ma, Y. Zhou, N. Li, M. Li, and P. Lu, "Attosecond control of correlated electron dynamics in strong-field nonsequential double ionization by parallel two-color pulses," Opt. Laser Technol. **108**, 235-240 (2018).
14. D. Wang, X. Zhu, L. Li, X. Zhang, X. Liu, P. Lan, and P. Lu, "Momentum gate for tunneling electrons with a circularly polarized control field," Phys. Rev. A **98**, 053410 (2018).
15. A. Schiffrin, T. Paasch-Colberg, N. Karpowicz, V. Apalkov, D. Gerster, S. Mühlbrandt, M. Korbman, J. Reichert, M. Schultze, S. Holzner, J. V. Barth, R. Kienberger, R. Ernstorfer, V. S. Yakovlev, M. I. Stockman, and F. Krausz, "Optical-filed-induced current in dielectrics," Nature (London) **493**, 70-74 (2013).
16. O. Schubert, M. Hohenleutner, F. Langer, B. Urbanek, C. Lange, U. Huttner, D. Golde, T. Meier, M. Kira, S. W. Koch, and R. Huber, "Sub-cycle control of terahertz high-harmonic generation by dynamical Bloch oscillation," Nat. Photon. **8**, 119-123 (2014).
17. L. Li, P. Lan, X. Liu, L. He, X. Zhu, O. D. Mücke, and P. Lu, "Method for direct observation of Bloch oscillations in semiconductors," Opt. Express **26**, 23844-23853 (2018).
18. M. Lein, "Attosecond probing of vibrational dynamics with high harmonic generation," Phys. Rev. Lett. **94**, 053004 (2005).
19. S. Baker, J. S. Robinson, C. A. Haworth, H. Teng, R. A. Smith, C. C. Chirilă, M. Lein, J. W. G. Tisch, and J. P. Marangos, "Probing proton dynamics in molecules on an attosecond time scale," Science **312**, 424-427 (2006).
20. P. Lan, M. Ruhmann, L. He, C. Zhai, F. Wang, X. Zhu, Q. Zhang, Y. Zhou, M. Li, M. Lein, and P. Lu, "Attosecond probing of nuclear dynamics with trajectory-resolved high-harmonic spectroscopy," Phys. Rev. Lett. **119**, 033201 (2017).
21. B. Wang, L. He, F. Wang, H. Yuan, X. Zhu, P. Lan, and P. Lu, "Resonance enhanced high-order harmonic generation in H_2^+ by two sequential laser pulses," Opt. Express **25**, 17777-17787 (2017).
22. B. Wang, L. He, F. Wang, H. Yuan, X. Zhu, P. Lan, and P. Lu, "Resonance-modulated wavelength scaling of high-order-harmonic generation from H_2^+," Phys. Rev. A **97**, 013417 (2018).
23. X.-B. Bian and A. D. Bandrauk, "Probing nuclear motion by frequency modulation of molecular high-order harmonic generation," Phys. Rev. Lett. **113**, 193901 (2014).
24. M. Li, G. Jia, and X.-B. Bian, "Alignment dependent ultrafast electron-nuclear dynamics in molecular high-order harmonic generation," J. Chem. Phys. **146**, 084305 (2017).
25. L. He, Q. Zhang, P. Lan, W. Cao, X. Zhu, C. Zhai, F. Wang, W. Shi, M. Li, X. Bian, P. Lu, and A. D. Bandrauk, "Monitoring ultrafast vibrational dynamics of isotopic molecules with frequency modulation of high-order harmonics," Nat. Commun. **9**, 1108 (2018).
26. H. J. Wörner, J. B. Bertrand, D. V. Kartashov, P. B. Corkum, and D. M. Villeneuve, "Following a chemical reaction

Optics EXPRESS

using high-harmonic interferometry," Nature (London) **466**, 604-607 (2010).
27. J. Chen, K. Wang, H. Long, X. Han, H. Hu, W. Liu, B. Wang, and P. Lu, "Tungsten disulfide-gold nanohole hybrid metasurfaces for nonlinear metalenses in the visible region," Nano Lett. **18**, 1344-1350 (2018).
28. D. Shafir, H. Soifer, B. D. Bruner, M. Dagan, Y. Mairesse, S. Patchkovskii, M. Yu. Ivanov, O. Smirnova, and N. Dudovich, "Resolving the time when an electron exits a tunnelling barrier," Nature (London) **485**, 343-346 (2012).
29. S. Ke, D. Zhao, Q. Liu, and W. Liu, "Adiabatic transfer of surface plasmons in non-Hermitian graphene waveguides," Opt. Quantum Electron. **50**, 393 (2018).
30. A. Fleischer, O. Kfir, T. Diskin, P. Sidorenko, and O. Cohen, "Spin angular momentum and tunable polarization in high-harmonic generation," Nat. Photonics **8**, 543-549 (2014).
31. Q. Liu, S. Ke, and W. Liu, "Mode conversion and absorption in an optical waveguide under cascaded complex modulations," Opt. Quantum Electron. **50**, 356 (2018).
32. C. Qin, L. Yuan, B. Wang, S. Fan, and P. Lu, "Effective electric-field force for a photon in a synthetic frequency lattice created in a waveguide modulator," Phys. Rev. A **97**, 063838 (2018).
33. M. Lewenstein, P. Balcou, M. Y. Ivanov, A. L'Huillier, and P. B. Corkum, "Theory of high-harmonic generation by low-frequency laser fields," Phys. Rev. A **49**, 2117-2132 (1994).
34. P. B. Corkum, "Plasma perspective on strong field multiphoton ionization," Phys. Rev. Lett. **71**, 1994-1997 (1993).
35. A. Baltuška, T. Udem, M. Uiberacker, M. Hentschel, E. Goulielmakis, C. Gohle, R. Holzwarth, V. S. Yakovlev, A. Scrinzi, T. W. Hänsch, and F. Krausz, "Attosecond control of electronic process by intense light fields," Nature (London) **421**, 611-615 (2003).
36. M. Nisoli, G. Sansone, S. Stagira, S. De Silvestri, C. Vozzi, M. Pascolini, L. Poletto, P. Villoresi, and G. Tondello, "Effects of carrier-envelope phase differences of few-optical-cylce light pulses in single-shot high-order-harmonic spectra," Phys. Rev. Lett. **91**, 213905 (2003).
37. C. Ott, M. Schönwald, P. Raith, A. Kaldun, G. Sansone, M. Krüger, P. Hommelhoff, Y. Patil, Y. Zhang, K. Meyer, M. Laux, and T. Peifer, "Strong-field spectral interferometry using the carrier-envelope phase," New J. Phys. **15**, 073031 (2013).
38. C. A. Haworth, L. E. Chipperfield, J. S. Robinson, P. L. Knight, J. P. Marangos, and J. W. G. Tisch, "Half-cycle cutoffs in harmonic spectra and robust carrier-envelope phase retrieval," Nat. Phys. **3**, 52-57 (2007).
39. N. Ishii, K. Kaneshima, K. Kitano, T. Kanai, S. Watanabe, and J. Itatani, "Carrier-envelope phase-dependent high harmonic generation in the water window using few-cycle infrared pulses," Nat. Commun. **5**, 3331 (2014).
40. E. Mansten, J. M. Dahlström, J. Mauritsson, T. Ruchon, A. L'Huillier, J. Tate, M. B. Gaarde, P. Eckle, A. Guandalini, M. Holler, F. Schapper, L. Gallmann, and U. Keller, "Spectral signature of short attosecond pulse trains," Phys. Rev. Lett. **102**, 083002 (2009).
41. M. Lein, N. Hay, R. Velotta, J. P. Marangos, and P. L. Knight, "Role of the intramolecular phase in high-harmonic generation," Phys. Rev. Lett. **88**, 183903 (2002).
42. T. Kanai, S. Minemoto, and H. Sakai, "Quantum interference during high-order harmonic generation from aligned molecules," Nature (London) **435**, 470-474 (2005).
43. O. Smirnova, Y. Mairesse, S. Patchkovskii, N. Dudovich, D. Villeneuve, P. Corkum, and M. Y. Ivanov, "High harmonic interferometry of multi-electron dynamics in molecules," Nature (London) **460**, 972-977 (2009).
44. P. M. Kraus, D. Baykusheva, and H. J. Wörner, "Two-pulse field-free orientation reveals anisotropy of molecular shape resonance," Phys. Rev. Lett. **113**, 023001 (2014).
45. T. Zuo and A. D. Bandrauk, "Charge-resonance-enhanced ionization of diatomic molecular ions by intense lasers," Phys. Rev. A **52**, R2511-R2514 (1995).
46. T. Seideman, M. Y. Ivanov, and P. B. Corkum, "Role of electron localization in intense-field molecular ionization," Phys. Rev. Lett. **75**, 2819-2822 (1995).
47. K. C. Kulander, F. H. Mies, and K. J. Schafer, "Model for studies of laser-induced nonlinear processes in molecules," Phys. Rev. A **53**, 2562-2570 (1996).
48. K. Liu, W. Hong, Q. Zhang, and P. Lu, "Wavelength dependence of electron localization in the laser-driven dissociation of H_2^+," Opt. Express **19**, 26359-26369 (2011).
49. L. Medišauskas, J. Wragg, H. V. D. Hart, and M. Y. Ivanov, "Generating isolated elliptically polarized attosecond pulses using bichromatic counterrotating circularly polarized laser fields," Phys. Rev. Lett. **115**, 153001 (2015).
50. K. Varjú, Y. Mairesse, B. Carré, M. B. Gaarde, P. Johnsson, S. Kazamias, R. López-Martens, J. Mauritsson, K. J. Schafer, P. Balcou, A. L'huillier, and P. Salières, "Frequency chirp of harmonic and attosecond pulses," J. Mod. Opt. **52**, 379-394 (2005).
51. B. Major, E. Balogh, K. Kovács, S. Han, B. Schütte, P. Weber, M. J. J. Vrakking, V. Tosa, A. Rouzée, and K. Varjú, "Spectral shifts and asymmetries in mid-infrared assisted high-order harmonic generation," J. Opt. Soc. Am. B **35**, A32-A38 (2018).
52. A. D. Bandrauk, S. Chelkowski, and H. S. Nguyen, "Attosecond localization of electrons in molecules," Int. J. Quantum Chem. **100**, 834-844 (2004).
53. P. Dietrich, M. Y. Ivanov, F. A. Ilkov, and P. B. Corkum, "Two-electron dissociative ionization of H_2 and D_2 in infrared laser fields," Phys. Rev. Lett. **77**, 4150-4153 (1996).
54. R. E. F. Silva, P. Rivière, F. Morales, O. Smirnova, M. Ivanov, and F. Martín, "Even harmonic generation in isotropic media of dissociating homonuclear molecules," Sci. Rep. **6**, 32653 (2016).
55. F. Morales, P. Rivière, M. Richter, A. Gubaydullin, M. Y. Ivanov, O. Smirnova, and F. Martín, "High harmonic

Optics EXPRESS

spectroscopy of electron localization in the hydrogen molecular ion," J. Phys. B: At. Mol. Opt. Phys. **47**, 204015 (2014).
56. M. Lara-Astiaso, R. E. F. Silva, A. Gubaydullin, P. Rivière, C. Meier, and F. Martín, "Enhancing high-order harmonic generation in light molecules by using chirped pulses," Phys. Rev. Lett. **117**, 093003 (2016).
57. M. F. Ciappina, J. A. Pérez-Hernández, A. S. Landsman, T. Zimmermann, M. Lewenstein, L. Roso, and F. Krausz, "Carrier-wave Rabi-flopping signatures in high-order harmonic generation for alkali atoms," Phys. Rev. Lett. **114**, 143902 (2015).
58. F. Giammanco, A. Pirri, F. Brandi, M. Barkauskas, and W. Ubachs, "Measurements of chirp-induced frequency shift in high-order harmonic generation in xenon," Laser Phys. **15**, 328-333 (2005).
59. J. Levespue, D. Zeidler, J. P. Marangos, P. B. Corkum, and D. M. Villenuve, "High harmonic generation and the role of atomic orbital wave functions," Phys. Rev. Lett. **98**, 183903 (2007).
60. A. D. Shiner, C. Trallero-Herrero, N. Kajumba, H.-C. Bandulet, D. Comtois, F. Légaré, M. Giguère, J.-C. Kieffer, P. B. Corkum, and D. M. Villeneuve, "Wavelength scaling of high harmonic generation efficiency," Phys. Rev. Lett. **103**, 073902 (2009).
61. D. Baykusheva, M. S. Ahsan, N. Lin, and H. J. Wörner, "Bicircular high-harmonic spectroscopy reveals dynamical symmetries of atoms and molecules," Phys. Rev. Lett. **116**, 123001 (2016).